

## Influence of Heat Treatment on the Mechanical Properties and Precipitation Kinetic of Sugar Palm Fiber Ash Reinforced LM26 Al Matrix Composites

Isah Aliyu<sup>1,2</sup>, Mohd Sapuan Salit<sup>1,3\*</sup>, Edi Syams Zainudin<sup>1,3</sup>, Mohd Zuhri Mohamed Yusoff<sup>1,3</sup> and Ridwan Yahaya<sup>4</sup>

<sup>1</sup>Advanced Engineering Materials and Composites Research Centre (AEMC), Department of Mechanical and Manufacturing Engineering, Universiti Putra Malaysia (UPM), 43400 Serdang, Selangor, Malaysia

<sup>2</sup>Department of Metallurgical Engineering, Waziri Umaru Federal Polytechnic, Birnin Kebbi, 860101, Nigeria

<sup>3</sup>Laboratory of Biocomposite Technology, Institute of Tropical Forestry and Forest Products, Universiti Putra Malaysia (UPM), 43400 Serdang, Selangor, Malaysia

<sup>4</sup>Science and Technology Research Institute for Defence (STRIDE), 43400, Kajang, Selangor, Malaysia

### ABSTRACT

Heat treatment is a commonly known treatment subjected to aluminum alloy and their composites to improve their mechanical properties for automotive, aerospace, and marine applications. The heat treatment was carried out to determine the influence of aging time and temperature on the mechanical properties of LM26 Al alloy reinforced with 0, 2, 4, 6, 8, and 10 wt% sugar palm fiber ash (SPFA) and its precipitation kinetics. The LM26 Al/SPFA composites were fabricated through the stir casting technique, solutionized at 500°C for 2 h, and quenched in water at room temperature. The quenched composites were aged at various ageing times and temperatures and allowed to air cool. The hardness, impact energy, tensile, and compression strengths of the aged composites were appraised. In addition, the precipitation kinetics were studied to validate the precipitation temperatures of LM26 Al matrix composites. The hardness of the composites increased with aging time

and temperature, with LM26 Al/10 wt% SPFA composite reaching a hardness peak of 102.10 VH at an aging temperature of 180°C after 5 h, compared to 56.70 VH for LM26 Al alloy. Similarly, after 5 h of aging at 180°C, the LM26 Al/8 wt% SPFA composite achieved maximum tensile and compression strengths of 198.21 MPa and 326.22 MPa, respectively. Precipitation temperature decreased from 584.8°C (LM26 Al alloy)

### ARTICLE INFO

#### Article history:

Received: 25 October 2022

Accepted: 25 January 2023

Published: 03 October 2023

DOI: <https://doi.org/10.47836/pjst.31.6.12>

#### E-mail addresses:

engalisa@yahoo.com (Isah Aliyu)

sapuan@upm.edu.my (Mohd Sapuan Salit)

edisyam@upm.edu.my; edisyam@gmail.com (Edi Syams Zainudin)

zuhri@upm.edu.my (Mohd Zuhri Mohamed Yusoff)

adr266@gmail.com (Ridwan Yahaya)

\* Corresponding author

to 480.46°C (LM26/ 10wt% SPFA), indicating that adding SPFA improved precipitation kinetics. The age-hardened composite with high hardness, tensile strength, and compression strength makes it a promising piston material application in the automotive industry.

*Keywords:* Aging time, LM26 Al alloy, mechanical properties, precipitation kinetics, sugar palm fiber

---

## INTRODUCTION

Metal matrix composites (MMCs) are becoming more popular due to their superior mechanical characteristics over monolithic metals. Aluminum matrix composites (AMCs) have been widely used to replace conventional and monolithic materials in various applications as lightweight structural materials due to their low density, superior creep resistance, high specific strength, excellent malleability, and excellent damping capacity, making them suitable for use in aerospace, electronics, marine, constructions, medical and automotive industries (Varalakshmi et al., 2019; Yuan et al., 2019; Yuan et al., 2017). AMCs have been widely used in various industrial applications, including medical components, automotive components for the production of pistons, brake discs, connecting rods, and aerospace components that include wings and fuselages (Bushlya et al., 2017; Chauhan et al., 2021; Ramasamy et al., 2021).

AMCs are strengthened by reinforcing them with either particles, fibers, or whiskers materials, which act as load-bearing materials. The commonly hard ceramic reinforcement materials used in the fabrication of AMCs include  $B_4C$ , SiC,  $MoS_2$ , and  $Al_2O_3$ , while fiber ashes used include rice husk (Olusesi & Udoeye, 2021), coconut shell (Babu et al., 2020), sugarcane bagasse (Kawin et al., 2020), bamboo leaf (Olaniran et al., 2019), bean pod (Bawa et al., 2020), groundnut shell (Venkatesh et al., 2019), and palm kernel shell (Iyasele, 2018) for strengthening purposes.

The sugar palm tree (*Arenga Pinnata* (Wurmb) Merr.) is a multifunctional tree that belongs to the family of palmea and is mostly found in countries such as Malaysia, China, and Indonesia. The sugar palm tree has dark braided fibers generally weaved from the bottom to the top of its trunk. Sugar palm fiber has many advantages and qualities, including less effort in preparing the fiber with high durability without any secondary processes and good seawater properties, which is suitable for the construction of ropes for ship cordage (Edhirej et al., 2017; Harussani & Sapuan, 2022; Ishak, Leman, et al., 2013). Other applications include shelters for fish breeding, road constructions, roofing materials, cushioning, weaving mats and hats, and making ropes and brooms (Ilyas et al., 2018; Ishak, Sapuan, et al., 2013). The preliminary studies showed that SPFA contained a high amount of refractory materials ( $SiO_2$ , CaO,  $Fe_2O_3$ ,  $Al_2O_3$ ). Agricultural waste contains a high amount of refractory materials, such as  $SiO_2$ , CaO,  $Fe_2O_3$ , and  $Al_2O_3$ , which account for their use as reinforcement material in AMCs (Ikubanni et al., 2022).

In order to achieve greater desirable mechanical properties of AMCs, the selection of good geometry of the reinforcement, such as size, shape, and quantity, is of paramount

importance. The reinforcement in the form of particles has been considered a new technological breakthrough in the fabrication of AMCs (Mabuwa et al., 2022). Selecting suitable reinforcing material and matrix is crucial for achieving the desirable properties of AMCs (Pasha et al., 2022). Moreover, homogeneous dispersion of reinforcement contents in the matrix and fabrication route employed, such as squeeze casting, stir casting, powder metallurgy, chemical vapor deposition pressure infiltration, solid solution precipitation hardening, and other metallurgical techniques, play a significant role in the improvement of the mechanical properties (Sajjadi et al., 2011; Samal et al., 2020; Vencl et al., 2010). Powder metallurgy and stir casting techniques are the most prevalent fabrication routes employed in the production of AMCs due to their cost effectiveness, ease of handle, greater hardness, and refined microstructural grains as compared to other methods (K. Singh et al., 2022; P. Singh et al., 2021; Reddy et al., 2020).

Stir casting eventually reduces the cost of producing AMCs by one-third to half compared to other methods, and the cost of high-volume fabrication decreased by one-tenth (Hashim et al., 1999; Yashpal et al., 2017). Stir casting is an advanced technique that involves stirring the molten metal to ensure uniform distribution of reinforcement before casting it into a prepared mold. The stirring action promotes vortex formation and increases reinforcement wettability with the matrix, thereby improving the bonding between the reinforcement and the matrix (Chak et al., 2020; Shaikh et al., 2019; Natrayan et al., 2017; V. K. Singh et al., 2015; Yuan et al., 2019). Many researchers are now using stir casting mostly in the fabrication of AMCs (Lokesh et al., 2022; Nambiar et al., 2020; Patel et al., 2022; Pasupulla et al., 2022; Velavan et al., 2020). Morampudi et al. (2022) fabricated an AA6061 aluminum matrix composite by reinforcing it with ilmenite ( $\text{FeTiO}_3$ ). Kennedy and Raja (2022) employed the stir casting technique to compare the mechanical characteristics of Al- $\text{B}_4\text{C}$  and Al-SiC composites, with Al- $\text{B}_4\text{C}$  composite having higher tensile and yield strength compared to Al-SiC composite.

LM26 aluminum alloy (Al-Si-Mg casting alloy) is widely used in the fabrication of block engines, pistons, intake manifolds, brake calipers, cylinder blocks, impellers, pumps, and cylinder heads valve components owing their overall performance of high specific-strength, better castability, low thermal expansion coefficient, improve wear resistance, adequate wettability, and superior corrosion resistance (Hiremath & Hemanth, 2018; Nagaraja et al., 2021; G. Singh & Sharma, 2021). When combined with proper heat treatment, the presence of Si and Mg in LM26 aluminum alloy led to the formation of  $\text{Mg}_2\text{Si}$  precipitates, eventually improving the mechanical properties significantly. The precipitation sequence of AMCs is given as supersaturated solid solution (SSSS), Guinier-Preston (GP) zone,  $\beta''$ ,  $\beta'$ , and  $\beta$  precipitates. The age-hardening response of LM26 Al alloy is influenced by many factors, such as chemical composition, solution heat treatment time and temperature, and aging time and temperature, all of which influence mechanical characteristics (Koppad et al., 2020).

Heat treatment, as a hardening process, is applied to metallic materials to improve their mechanical, structural, and physical properties for engineering applications (Somasekhar et al., 2018). Heat treatment resulted in precipitation hardening and improved mechanical properties compared to non-heat-treated AMCs. Heat-treated AMCs were found to have better mechanical characteristics, as well as reduced wear rate, than non-heat-treated AMCs (Mistry & Gohil, 2019).

The influence of aging temperature on wear and mechanical characteristics of the A375 matrix reinforced with large and small-sized SiC particles was investigated by Lakshmikanthan et al. (2020). The reinforcement of fly ash and graphite was uniformly distributed in the matrix of A6061 after T6 treatment with improved mechanical characteristics (B. Singh et al., 2022). The influence of aging temperature on the mechanical characteristics of Al-Si alloy and Al-Si/6% fly ash matrix composite was investigated by Tiwari et al. (2017). The temperatures under consideration for aging were 130°C, 150°C, 175°C, and 200°C. Peak hardness, tensile, and impact strengths were noticed in the alloy and composite at 175°C of aging temperature. Sharma et al. (2019) investigated the influence of T4 and T6 treatment on the wear behavior of Al-based composites and discovered that the wear rate improved with a lower coefficient of friction of T6-treated composites compared to T4-treated and as-cast composites. Sam et al. (2020) studied the effect of T6 treatment compared to TiB<sub>2</sub>, WC, and ZrO<sub>2</sub> as reinforcements on the tribological and mechanical characteristics of LM 25 aluminum alloy. They discovered that incorporating WC as reinforcement significantly improved the hardness and tensile strength of the composites after T6 heat treatment, with a corresponding lower wear rate than incorporating TiB<sub>2</sub> and ZrO<sub>2</sub> as reinforcement. Li et al. (2018) investigated the tribological behavior of Al-5% Si-1.0% Cu-0.5% Mg matrix reinforced with SiC particles by subjecting it to heat treatment. They discovered that after heat treatment, the composite had a lower wear rate and lower coefficient of friction than the base alloy.

The depletion of mineral resources such as synthetic reinforcements, with their high cost, high weight, and limited supply, are major setbacks in most developing countries in the fabrication of AMCs (Ikumapayi et al., 2022; Seetharaman et al., 2022). The reliance on importing synthetic materials from overseas and the high cost of foreign exchange implies that synthetic materials purchased locally are relatively expensive if available. Researchers have shown kin interest in improving the mechanical characteristics of AMC by incorporating cheaper and readily available green reinforcements into AMCs (Khan et al., 2022). According to the literature and to the best of the authors' knowledge, the study of heat treatment on the mechanical behavior and precipitation kinetics of LM26 AMCs reinforced with SPFA has not been explored and requires investigation. This research aims to determine the appropriate aging time and temperature corresponding to optimal hardness, impact energy, tensile, and compression strength, as well as the effect of precipitation temperature on the precipitation kinetics of the LM26 Al/SPFA composite.

## MATERIALS AND METHODS

### Material Preparation

The matrix material used in this investigation was LM26 Al alloy, with a chemical composition of 9.70% Si, 2.40% Cu, 1.2% Mg, 1.10% Fe, 0.91% Zn, 0.83% Ni, 0.50% Mn, 82.86% Al, and 0.50% of other elements. Sugar palm fiber was collected from Jempol, Negeri Sembilan, Malaysia, and used as reinforcement. The sugar palm fiber was washed under running tap water and dried in the laboratory for 48 h before being burnt in an incinerator to produce sugar palm fiber ash (SPFA). The SPFA was collected and heated in an electrical muffler furnace for 4 h at 700°C to remove the volatile and carbonaceous constituents. After being screened with sieve sets arranged in descending order of finest, the SPFA with an average size of less than 75 µm was used, and its chemical composition was analyzed with X-ray fluorescence (SHIMADZU, EDX-720) as shown in Table 1.

Table 1  
*Elemental constituent of LM26 Al-alloy*

| Elements        | Si   | Mg   | Cu   | Fe   | Mn   | Zn   | Ni   | Others | Al   |
|-----------------|------|------|------|------|------|------|------|--------|------|
| % mass fraction | 9.70 | 1.20 | 2.40 | 1.10 | 0.50 | 0.91 | 0.83 | 0.50   | Bal. |

The composites were fabricated by using a stir-casting route. The LM26 Al alloy was cut into pieces, placed in the graphite crucible of an induction electrical resistance furnace, and heated above 700°C. After the LM26 Al alloy was completely melted, followed by manually stirring and allowed to cool to a semi-solid state at 580°C. SPFA were preheated in a muffler furnace (up to 500°C) to remove moisture and improve wettability. The preheated SPFA and 1wt% Mg were introduced into the molten LM26 Al alloy vortex to improve its wettability. The molten mixture was stirred for 10 min at 500 rpm to ensure proper reinforcement mixing in the base matrix. After stirring, the molten mixture was degassed with 1% hexachloroethane (C<sub>2</sub>Cl<sub>6</sub>) powder. Then, the mixture was poured into a precast sand mold to produce a standard tensile strength specimen in accordance with ASTM E 8 (ASTM International, 2015). The procedure described was used to produce composites with varying percentages of SPFA content ranging from 0 to 10wt% at 2wt% intervals. There were nine tensile samples made from each composition.

### Heat Treatment Processes

The fabricated LM26 Al alloy and LM26 Al-SPFA composites were packed in a resistance heat treatment furnace, and solution heat treatment (SHT) was carried out at 500°C for 2 h before quenching in water (at room temperature). The quenched samples were divided into three parts to analyze their hardness, impact energy, tensile strength, compression strength, and precipitation kinetic of the AMCs.

One tensile sample, each from the same composition from SHT and quenched samples was machined into eleven hardness samples in accordance with ASTM E383 (ASTM International, 2017).

To determine the aging temperature with peak hardness, five quenched SHT hardness samples, each from the same composition, were aged in the furnace for 2 h, one each at temperatures of 90°C, 120°C, 150°C, 180°C, and 210°C before being cooled at room temperature. Similarly, six quenched SHT hardness samples, each from the same compositions, were aged in the furnace at 180°C, one each for different aging times of 1 h, 2 h, 3 h, 4 h, 5 h, and 6 h, cool outside the furnace in still air to determine the aging time that corresponds to peak hardness.

Three sets each of the same composition of tensile and compression strengths samples from the quenched SHT were aged at 180°C for 5 h and air cool to determine the impact energy, tensile strength, and compression strength.

The SHT and quenched samples containing SPFA content of 0, 2wt%, 8wt%, and 10wt% were filed to obtain 6 mg of powder for the study of precipitation kinetic.

### **X-ray Diffraction**

The X-ray diffraction (PANalytical X'Pert Pro Model: PW3040/60, Netherlands) with Cu-K $\alpha$  radiation, wavelength ( $\lambda$ ) of 1.5406 Å, in an angle range of  $2\theta = (4^\circ-90^\circ)$  working at the rate of 2 °/min was utilized to ascertain the oxides and intermetallic compounds in SPFA, as-cast LM26 Al alloy and LM26 AMCs reinforce with SPFA.

### **Hardness Test**

Micro hardness testing was carried out by using a digital Mirco-vicker's hardness tester (Model: 401MVD, Germany) in accordance with ASTM E384 (ASTM International, 2017). Surface flaws were abraded with 400 grit to 1000 grit papers before being polished with 1200 grit emery cloth. After three indentations on each age-hardened sample, the average hardness values were recorded after the samples were subjected to a 1 kg load for 15 sec.

### **Standard Tensile and Compression Tests**

The tensile strength, compression strength, and impact energy tests were performed on the age-hardened LM26 alloy and its composite reinforced with SPFA. The ultimate tensile strength and compression strengths were evaluated on a computerized Universal Testing Machine (UTM) (Model: INSTRON M/c 5566) with a 100 kN capacity at a strain rate of 1.0 mm/min in accordance with the standard ASTM E-8 and E-9 (ASTM International, 2015a).

### **Impact Energy Test**

The impact energy testing was carried out using a Charpy impact machine of 300J capacity with a pendulum of striking speed of 5 m/s. The samples were machined into impact test specimens with dimensions of 55 mm × 10 mm × 10 mm, with a notch depth of 2 mm and a radius of notch tip 0.02 at 45° according to ASTM E23 standard (ASTM International, 2023). The impact test was performed on three tests of samples, with readings taken and their average values recorded.

### **Microstructural Analysis**

The morphology and EDS spectrum of the aged samples at 180°C for 5 h was characterized by using the scanning electron microscope (JSM 6400, JEOL Ltd, Tokyo, Japan) connected with energy dispersive X-ray spectroscopy (DES) according to ASTM standards E 407 and then, polished with different grades of emery papers according to standard metallographic procedure (ASTM International, 2015b). The samples were etched with Keller's reagent, composed of 95 ml of water, 2.5 ml HNO<sub>3</sub>, 1.5 ml HCl, and 1.0 ml HF, and then subjected to SEM analysis.

### **Differential Scanning Calorimetry (DSC)**

Differential scanning calorimetry (DSC) (Model: Mettler Toledo TGA/DSC HT 3, Swiss) was used to perform thermal analysis on LM26 AMC with SPFA content of 0, 2wt%, 8wt%, and 10wt%. The samples were filed to powder form after SHT at 500°C for 4 h and quenched in water. The 6mg of powder samples were weighed using an electronic balance (AND GF-1000, Model T0380263, Japan) and placed in a pan constructed on a framework in the DSC cell. An empty pure aluminum reference pan was positioned on a symmetric framework with its own constantan disc and chromel-alumel thermocouple beneath it. To minimize oxidation, the samples were heated at 10°C/min in a nitrogen atmosphere supplied at 50 mL/min between 500°C and 700°C. The sample temperature was measured with a chromel-alumel thermocouple, and the heat flow was calculated by comparing the difference in temperature between the composites and the reference pure aluminum. The data from all DSC runs were saved to the instrument memory.

## **RESULTS AND DISCUSSION**

### **X-ray Diffraction Patterns Analysis**

The XRD diffraction patterns of SPFA, LM26 Al-alloy, and fabricated LM26 Al-matrix/8wt% SPFA composite are depicted in Figure 1. The XRD confirmed the presence of SiO<sub>2</sub>, CaO, Fe<sub>2</sub>O<sub>3</sub>, and Al<sub>2</sub>O<sub>3</sub> in SPFA, as determined by XRF. Furthermore, SiO<sub>2</sub> was discovered to be the dominant constituent in SPFA. Similarly, the XRD of LM26 alloy

and LM26 Al/SPFA composite confirmed the presence of Al as the dominant and traces of Si and Mg in the form of  $Mg_2Si$  and  $Al_5FeSi$ . These intermetallic compounds,  $Mg_2Si$  and  $Al_5FeSi$ , formed an excellent bonding with the reinforcement (SPFA). It further validated SPFA as good reinforcing material in an LM26 Al alloy matrix. The major diffraction peak of SPFA is  $29.4^\circ$  with a crystallinity index of 52.76%. The matrix, LM26 Al alloy, has a crystallinity index of 49.75% with three major diffraction peaks of  $28.44^\circ$ ,  $38.44^\circ$ , and  $44.69^\circ$ , which are characteristics of metallic aluminum (Shaikh et al., 2019). The addition of SPFA into LM26 Al alloy caused a decrease in the crystallinity of the LM26 Al alloy to 28.97% with a corresponding major peak of  $38.37^\circ$ ,  $41.76^\circ$  and  $44.72^\circ$ .

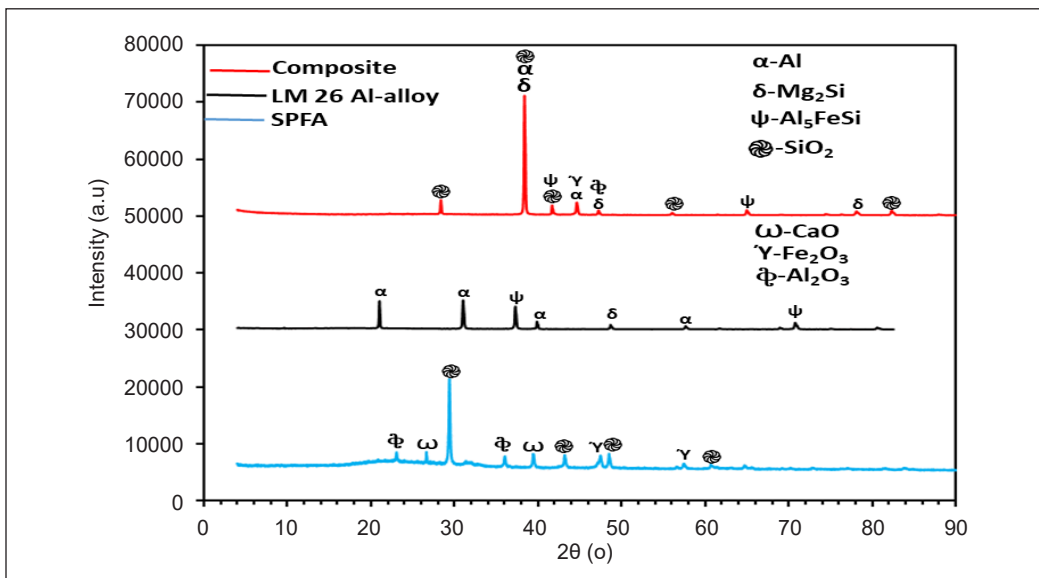


Figure 1. XRD of SPFA, LM26 Al alloy and LM26 Al/SPFA composite

### Hardness Behavior

Hardness testing was performed on the composites to investigate the effects of aging time and temperature. The fabricated composites had a maximum hardness value of 93.62 HV at 10wt% of SPFA addition.

The SHT at  $500^\circ C$  for 4 h and fast quenching in water led to the formation and retention of a supersaturated single phase, and aging the quenched sample at various temperatures allowed precipitation of the second phase to form, which was metastable. This small metastable precipitate impinged on dislocation movement, thereby increasing the hardness of the alloys and composites (Goudar et al., 2018).

Figure 2 depicts the hardness variation of heat-treated LM26 Al matrix/ (0-10wt%) SPFA composites aged for 2 h at  $90^\circ C$ ,  $120^\circ C$ ,  $150^\circ C$ ,  $180^\circ C$ , and  $210^\circ C$ . A study of aging temperature variation was carried out to determine the temperature that results in peak

hardness. It was evident that aging temperature affected the hardness of LM26 Al alloy and its composites (Figure 2). Figure 2 depicts the linear increase in hardness of LM26 Al alloy and its composites reinforced with SPFA with increasing aging temperature at an aging time of 2 h. The increase in hardness with increasing aging temperature could be due to an increase in the number of precipitated forms. The LM26 Al alloy and its composites reinforced with SPFA attained peak hardness after being aged to 180°C. Beyond the aging temperature of 180°C, the hardness of the LM26 Al alloy and its composites dropped due to softening caused by overheating at 210°C (Flanagan et al., 2019).

The hardness variation of age-hardened LM26 Al matrix (0–10wt%) SPFA composites at different aging times of 1 h, 2 h, 3 h, 4 h, 5 h, and 6 h at 180°C is shown in Figure 3. Since the peak hardness was observed at 180°C, this temperature setting was used to investigate the hardness of LM26 Al alloy and its composites over a range of aging times. Figure 3 shows the hardness values in a linear increment of aging times from 1 h to 5 h and then began to drop. The corresponding hardness values of LM26 Al alloy and its composites aged below the aging time of 4 h were lower than the fabricated LM26 Al alloy and its composites and were referred to as under-aged. The lower hardness values observed below 4 h were due to incomplete precipitate formation of the intermetallic compounds. Peak hardness was observed at 5 h (Figure 3) for LM26 Al alloy and its composites. Geetha and Ganesan (2015) reported that peak hardness was attained between 4 h and 6 h aging time. The peak hardness was achieved due to the formation of hard fine precipitate phases of intermetallic compounds ( $Mg_2Si$  and  $Al_3FeSi$ ) and uniformly dispersed SPFA (Figure 8e), which provided resistance to the indenter when indenting the surfaces of LM26 Al alloy and its composite. The precipitation of the intermetallic compounds was enhanced by heating the LM26 Al alloy and its composites to the desired temperature and allowing sufficient time to lapse (Rajasekaran et al., 2012). Figure 3 shows that increasing the aging time beyond 5 h caused a decrease in hardness due to the coarsening of the precipitate formed and its softening at 6 h, referred to as over-aged.

The hardness variation of aged hardened LM26 Al alloy and its composites reinforced with varied amounts of SPFA ranging from 0 to 10wt% in 2wt% intervals at aging times of 1 h, 2 h, 3 h, 4 h, and 5 h is shown in Figure 4. Regardless of the aging time, it was evident that the hardness values increased as the amount of SPFA increased. The increase in hardness values was due to the increase in hard refractory constituents of  $SiO_2$ ,  $Al_2O_3$ ,  $CaO$ , and  $Fe_2O_3$  present in SPFA as a result of its addition [Figure 8 (a-f)]. The hardness value of the aged hardened LM26 Al matrix/10wt% SPFA composite after 5 h was 9.06% higher than that of the fabricated composite counterpart. It was due to the precipitate formed after aging (Figure 8f). A peak hardness value of 102.1 VH was obtained with aged LM26 Al/10wt% of SPFA composite at 5 h and 180°C, while the lowest hardness value of 56.2 VH was achieved with LM26 Al alloy after 1 h aging at 180°C.

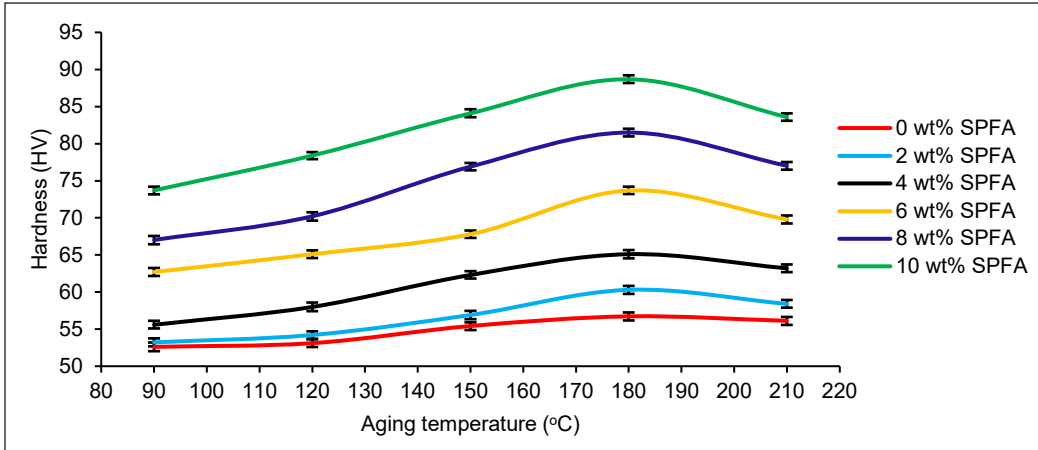


Figure 2. Hardness (VH) of composites at various aging temperatures

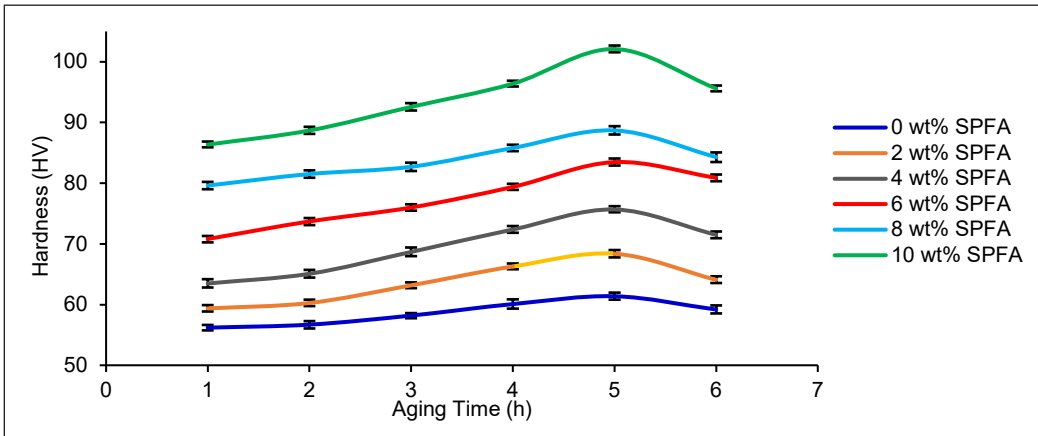


Figure 3. Hardness (VH) of composites at various aging times

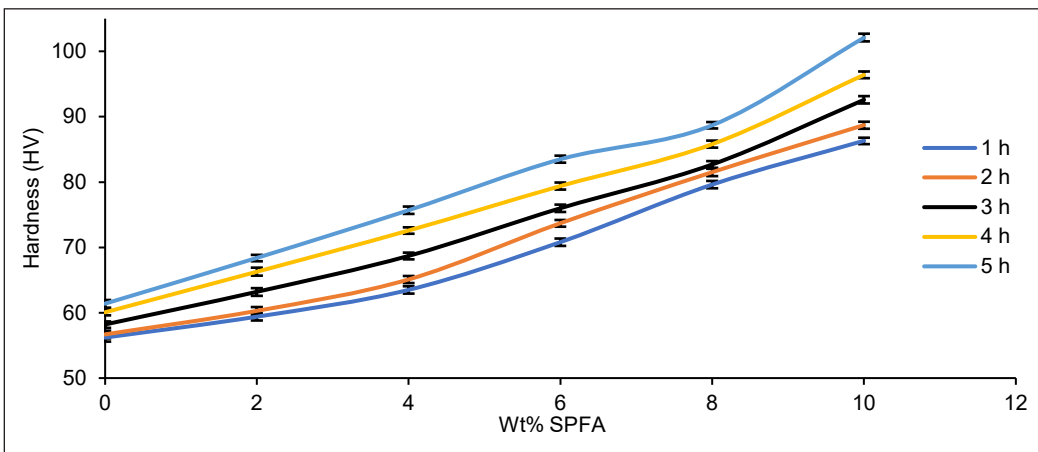


Figure 4. Hardness (VH) of composites at various reinforcement (SPFA) percentages

### Tensile Strength

The stress-strain curves of the materials after 5 h of aging at 180°C are presented in Figure 5. The variation of the volume fraction of reinforcement under tensile conditions was studied. The curves of the SPFA-reinforced composite differ significantly from those of the LM26 Al alloy. The addition of SPFA as reinforcement into the LM26 Al matrix, coupled with age hardening, increased the tensile strength of the composites. It could be explained by the homogeneous distribution of SPFA particles, precipitates that formed after aged hardening, and the SPFA particle's larger surface area within the matrix, which increased interface strength between the reinforcement and the material (Sabry et al., 2020). It was shown in Figure 5 that there was a critical SPFA content above or below which the tensile strength of the composites was lowered. The tensile strength of the composites is greatest when the amount of SPFA particles is up to 8 wt%; above and below this amount, the tensile strength is lowered. Similarly, Manda et al. (2021) reported improved tensile strength with adding molybdenum disulfide in AA6061 and coupled with aging at 180°C for 12 h. The agglomerates formed by the high concentration of SPFA up to 10 wt% act as stress concentration centers. The formation and distribution of the agglomerates within the LM26 Al alloy matrix cause a drop in the tensile strength of the ML26 Al/10 wt% SPFA composite (Al-Salihi & Judran, 2020).

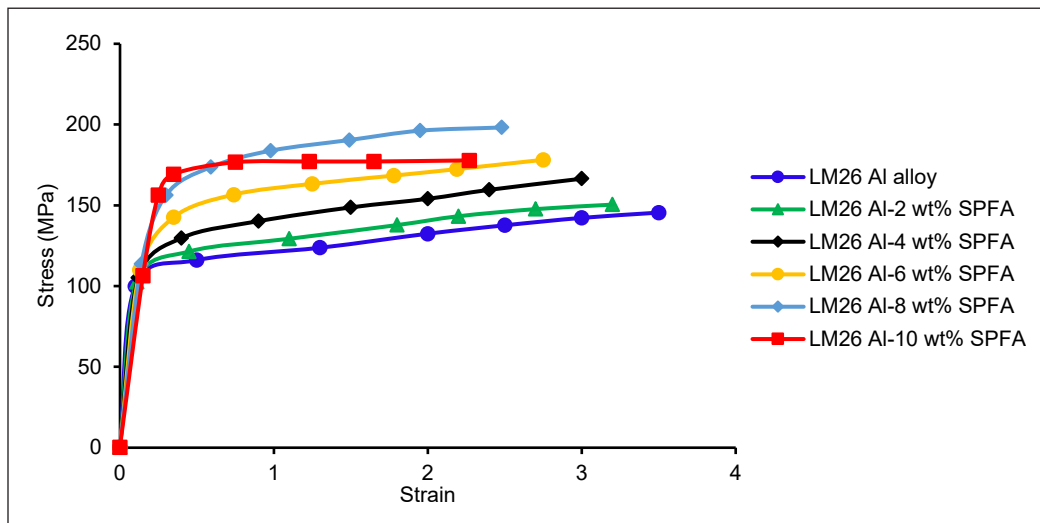


Figure 5. Stress-strain curve of LM26 Al alloy and composites with varying reinforcement content under tension

### Compression Strength

The stress-strain curves of the LM26 Al alloy and LM26 Al/SPFA composites aged at 180°C for 5 h after the compression test as depicted in Figure 6. There was a noticeable difference between the composites reinforced with SPFA and the LM26 Al alloy. The

compression strength of the SPFA-reinforced composite was improved significantly compared to the LM26 Al alloy. The compression strength of LM26 Al with 10 wt% SPFA composite is higher when compared with the composites having 2, 4, and 6 wt% SPFA. LM26 Al composite with 8 wt% SPFA was found to have the highest compression strength. The compression strength of the composites improved significantly with increased volume fraction of the SPFA reinforcement, and precipitates formed as a result of aging. An improvement of 24.36 % in the compression strength was noticed with 8 wt% SPFA reinforced LM26 Al matrix composite compared to the LM26 Al matrix alloy. A study by Das et al. (2019) reported an increase in compression strength with the incorporation of SiC in Al 7075 and aged at 483°C for 2 h compared to the as-cast. It is owing to the SPFA exhibiting a strong bond with LM26 Al matrix alloy, which assists in bearing more compression load as compared to LM26 Al matrix alloy. The increase in compression strength could also be due to increasing dislocation density at the reinforcement matrix interface and load transfer to the strongly bonded SPFA in the LM26 Al matrix (Khan et al., 2022; Rajaram et al., 2022). Similarly, the improvement in compression strength could be a result of a closed pack of the reinforcement in the matrix, the interfacial properties exhibited between the reinforcements and matrix, which are associated with wettability (Arunachalam et al., 2019; Kondoh et al., 2010).

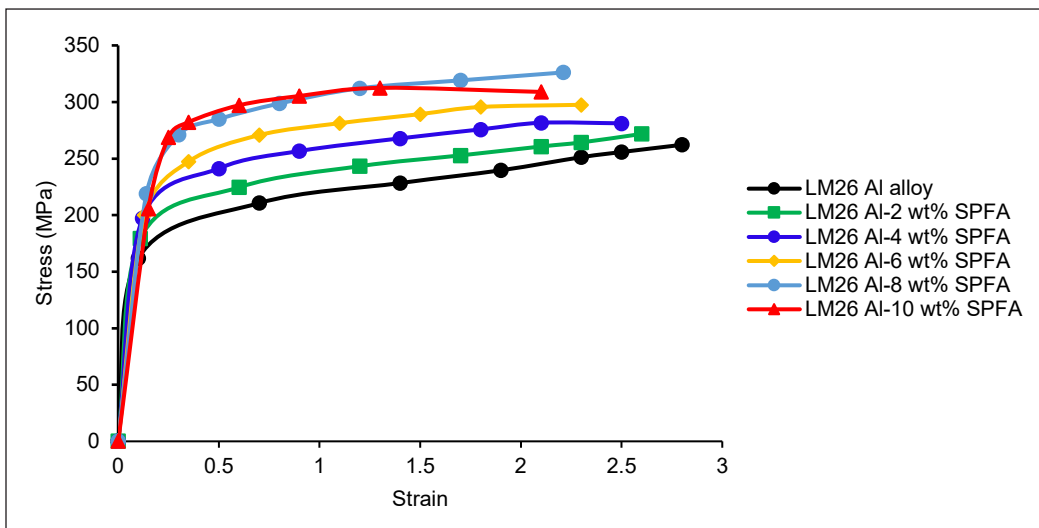


Figure 6. Stress-strain curve of LM26 Al alloy and composite with varying SPFA content under compression

### Impact Energy

An impact strength test was used to appraise the toughness of the composites. The Charpy impact testing was used to determine the energy absorbed by the composites in a single strike before braking. The impact energy of LM26 Al alloy decreased with the increase of

SPFA content to 10wt% SPFA (14.75 J to 6.98 J) (Figure 7). The drop in impact energy could be attributed to the change of ductile matrix of LM26 Al alloy to brittle LM26 Al/10 wt% SPFA composite by the addition of hard ceramic content of SiO<sub>2</sub>, CaO, Fe<sub>2</sub>O<sub>3</sub>, and Al<sub>2</sub>O<sub>3</sub>, present in the SPFA as confirmed by XRF (Table 1) (Manikandan & Arjunan, 2019). The toughness of a material is the amount of energy it absorbs before it fractures. The fracture toughness of LM26 Al alloy was high due to high plastic deformation. The fracture toughness decreased due to the presence of SPFA (SiO<sub>2</sub>, CaO, Fe<sub>2</sub>O<sub>3</sub>, and Al<sub>2</sub>O<sub>3</sub>), which led to a decrease in the plastic deformation energy

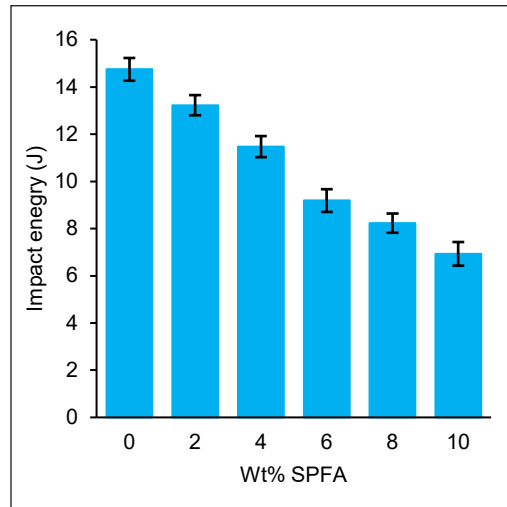


Figure 7. Variation of impact energy with SPFA for LM26 Al/SPFA composite aged for 5 h at 180°C

of the composites. A study by Kumar et al. (2018) reported a decrease in impact strength by incorporating coconut and zirconium oxide in Al 6082 base alloy.

### Microstructural Analysis of LM26 Alloy and LM26 Al/SPFA Composite

Figure 8 depicts the SEM morphology of (a) LM26 Al alloy, (b) LM26 Al/2 wt% SPFA, (c) LM26 Al/4 wt% SPFA, (d) LM26 Al/6 wt% SPFA, (e) LM26 Al/8 wt% SPFA, and (f) LM26 Al/10 wt% SPFA composites solutions at 500°C for 4 h, quenched in water, aged for 5 h at 180°C. The elements such as Al, Si, C, Mg, Fe, K, and O were identified in the elemental analysis of composites in Figure 8. Figure 8a shows the morphology of the alloy that consists of precipitates of intermetallic compounds formed due to aged hardening. The heat treatment transformed fibrous eutectic Si and Mg into fine spheroids uniformly distributed in the LM26 Al matrix. Fine globular eutectic Si and Mg particles were produced during heat treatment and could be seen in the alloy and composites (Figure 8a) (Yang et al., 2018).

Consequently, the heat treatment equally dissolved Mg<sub>2</sub>Si particles in the alloy and composites, leading to structural homogenization, fragmentation of Si particles, an increase in the number of Si particles, and coupling with SPFA particles, resulting in the composites being stronger compared to the corresponding fabricated alloy (Lakshmikanthan et al., 2020). SPFA particles were evenly dispersed in the LM26 Al matrix, as evidenced by all the micrographs (Figure 8 b–e). As shown in Figure 8(a–e) in the micrographs, the composites revealed excellent SPFA particle dispersion with no noticeable porosity or casting defects. However, in the case of the LM26 Al/10wt% SPFA composite, some agglomerates have

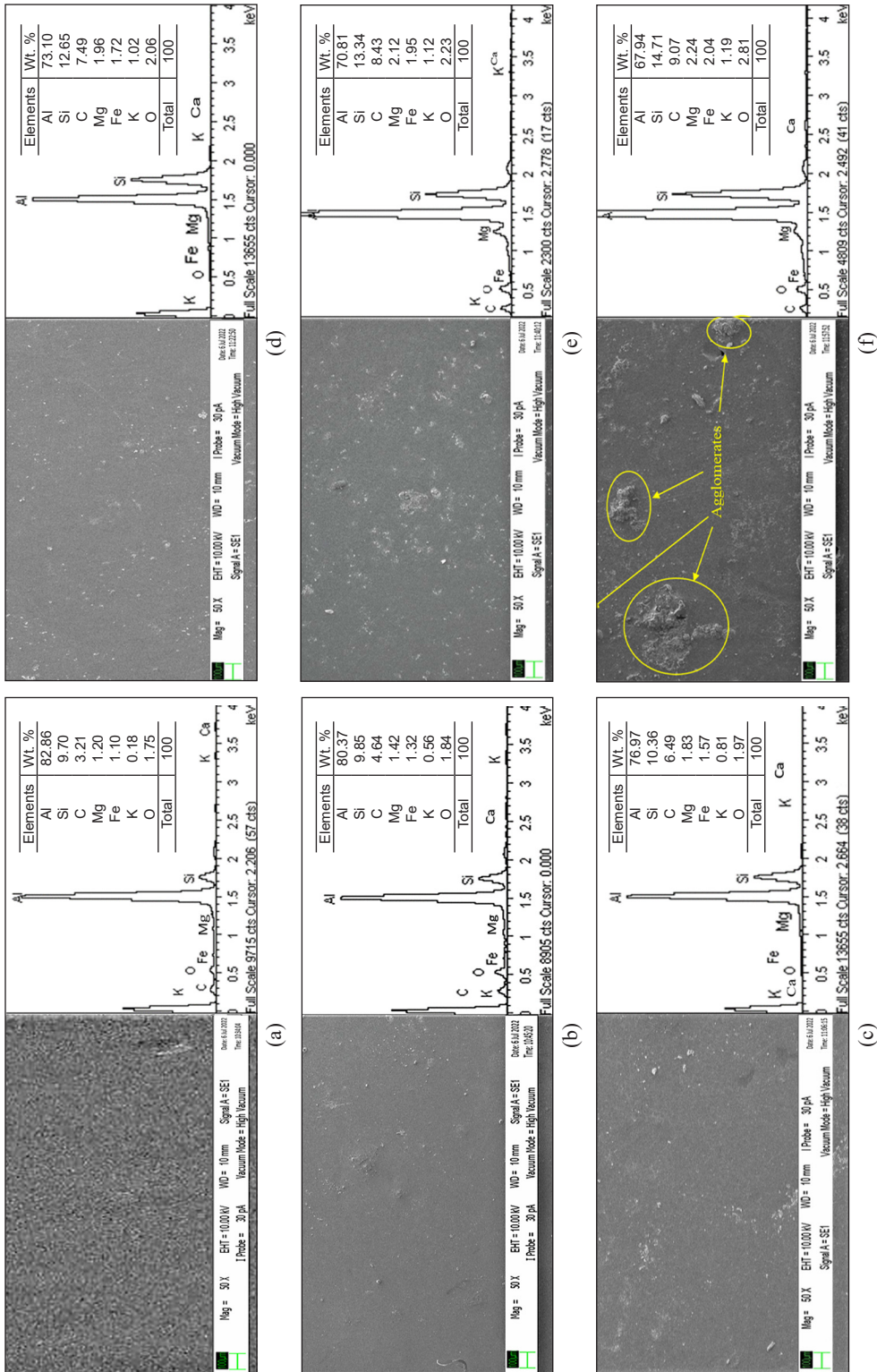


Figure 8. SEM morphology and EDS of age-hardened: (a) LM26 Al alloy, (b) LM26 Al/2 wt% SPFA, (c) LM26 Al/4 wt% SPFA, (d) LM26 Al/6 wt% SPFA, (e) LM26 Al/8 wt% SPFA and (f) LM26 Al/10 wt% SPFA aged for 5 h at 180°C

small SPFA (Figure 8f). SPFA particle agglomerate formation on a smaller scale was observed in a few spots in the LM26 Al/10wt% composite. Amongst all the composites, the overall dispersion of SPFA particles was reasonably uniform, with no notable casting defects such as porosity. The evenly distributed SPFA particles in the LM26 Al matrix alloy were due to the appropriate stir-casting parameters used during the composite fabrication.

### Differential Scanning Calorimeter (DSC)

The DSC thermogram was used to investigate the kinetics during precipitation or dissolution. In Al-Si-Mg alloys, supersaturated solid solution decomposed in the following order: From supersaturated solid solution  $\rightarrow$  Guinier-Preston (GP) zone (rich in Si)  $\rightarrow$   $\beta''$  precipitates  $\rightarrow$   $\beta'$  precipitates  $\rightarrow$   $\beta$  phase and Si particle (He et al., 2018; Rajasekaran et al., 2012; Xia et al., 2020). The DSC thermogram shown in Figure 9 depicted the thermal reactions of LM26 Al composites reinforced with 0, 2wt%, 8wt%, and 10wt% of SPFA at a heating rate of 10 °C/min from 500°C to 700°C in a vacuum with nitrogen gas flowing at a rate of 50 mL/min. The exothermic peaks that normally form indicating the formation of metastable GP zone after solution heat treatment and quenching, were completely absent. Between 550°C and 610°C, a series of endothermic peaks associated with  $\beta''$  and  $\beta'$  precipitates formation were observed from the DSC thermogram (Figure 9) for the samples. The similarities in the DSC curves that overlapped with SPFA addition implied that the precipitation sequence in the alloy was, to some extent, independent of the composition. The assertion was consistent with the  $\beta''$  precipitation formation findings of Fang et al. (2010).

As depicted in Figure 9, the endothermic peaks observed for the alloy and composites were temperature dependent, known as precipitation temperature, the transition temperature, and decreased with increasing percentage of SPFA addition (Table 2). A similar finding has been reported by Fröck et al. (2019). The area between the peaks in Figure 9, which decreased with an increase of SPFA (Table 2), represented the reaction enthalpy, which was proportional to the molar heat of the reaction and the volume fraction of the precipitating or dissolving phases. The corresponding precipitation temperatures were related to precipitate stability and reaction kinetics and decreased as SPFA increased (Table 2). From the DSC thermogram (Figure 9), it was observed that the  $\beta''$  and  $\beta'$  precipitate formation were lower in the composites compared to the matrix alloy. Adding SPFA into LM26 Al alloy decreased the temperature required to attain peak hardness. Therefore, the degree of accelerated precipitation kinetic of LM26 Al alloy was found as follows: LM26 Al + 10wt% SPFA > LM26 Al + 8wt% SPFA > LM26 Al + 2wt% SPFA > LM26 Al alloy. According to the DSC, adding SPFA particles as reinforcement improved aging kinetics, sped up phase transformation reaction, and acted as a seed for precipitation during the heat treatment process, resulting in significant alloy strengthening of the matrix material during the heat treatment process.

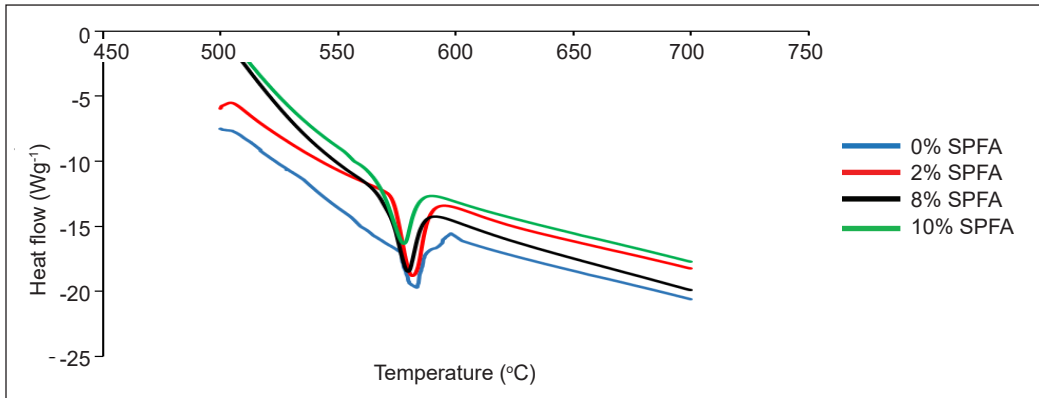


Figure 9. DSC thermogram of quenched LM26 Al matrix composite reinforced with 0, 2 wt%, 8 wt%, and 10 wt% SPFA

Table 2  
DSC characteristics of LM26 Al matrix and its composite reinforced with SPFA

| SPFA Content (%) | Precipitation temperature (°C) | Peaks area (Jg <sup>-1</sup> ) | Peak height (Wg <sup>-1</sup> ) | Peak width (°C) |
|------------------|--------------------------------|--------------------------------|---------------------------------|-----------------|
| 0                | 584.80                         | 378.26                         | 6.08                            | 9.42            |
| 2                | 583.98                         | 374.16                         | 6.05                            | 9.30            |
| 8                | 582.39                         | 332.03                         | 5.25                            | 8.71            |
| 10               | 580.46                         | 327.32                         | 4.68                            | 8.56            |

## CONCLUSION

Stir casting was used to fabricate SPFA successfully reinforced LM26 Al matrix composite, which was then solution heat treated and aged, and their mechanical properties and precipitation kinetics were studied. The most favorable heat treatment for LM26 Al/SPFA composites was the solution heat treated at 500°C for 4 h and aging treatment at 180°C for 5 h. The hardness of the LM26 Al/10 wt% SPFA composite (102.1 HV) increased by 80.07% after 5 h aging at 180 °C in compared to the LM26 Al alloy (56.7 HV). A peak tensile and compression strengths for LM26 Al/8 wt% SPFA composite of 198.21 MPa and 326.22 MPa, respectively was attained after aging at 180°C for 5 h compared to LM26 Al alloy corresponding to 145.46 MPa and 262.31 MPa. The impact energy of the LM26 Al alloy (14.75 J) dropped by 112.84% after 5 h aging at 180°C compared to the impact energy of the LM26 Al/10 wt% composite (6.93 J). The SEM morphology reveals uniform dispersion of SPFA in LM26 Al matrix composite, formation of precipitates after aging, and agglomerate formed is evidenced at a high loading of 10 wt% SPFA. The precipitate formed in the LM26 Al matrix was faster with increasing SPFA addition and occurred at a lower temperature. The precipitate formed after age-hardening was a major contributing factor leading to increased hardness of the aged composite compared to the as-cast composite.

## ACKNOWLEDGEMENT

The authors thank Universiti Putra Malaysia, Malaysia, and Waziri Umaru Federal Polytechnic in Birnin Kebbi, Nigeria. This research was supported financially by Universiti Putra Malaysia (GP/IPS/2021/9697100 and GP/IPS/2021/9702700).

## REFERENCES

- Al-Salihi, H. A., & Judran, H. K. (2020). Effect of Al<sub>2</sub>O<sub>3</sub> reinforcement nanoparticles on the tribological behaviour and mechanical properties of Al6061 alloy. *Materials Science*, 7(4), 486-498. <https://doi.org/10.3934/materci.2020.4.486>
- Arunachalam, R., Piya, S., Krishnan, P. K., Muraliraja, R., Christy, J. V., Mourad, A. I., & Al-Maharbi, M. (2019). Optimization of stir – squeeze casting parameters for production of metal matrix composites using a hybrid analytical hierarchy process - Taguchi-Grey approach. *Engineering Optimization*, 52(7), 1166-1183. <https://doi.org/10.1080/0305215X.2019.1639693>
- ASTM International. (2017). *Standard Test Method for Microindentation Hardness of Materials* (ASTM Standard Version E384-05A). <https://doi.org/10.1520/E0384-05A>
- ASTM International. (2015a). *Standard Test Methods for Tension Testing of Metallic Materials* (ASTM Standard Version E8/E8M- 13A). [https://doi.org/10.1520/E0008\\_E0008M-13A](https://doi.org/10.1520/E0008_E0008M-13A)
- ASTM International (2015b). *Standard Practice for Microetching Metals and Alloys* (ASTM Standard Version E384-05). <https://webstore.ansi.org/standards/astm/astme38405>
- ASTM International. (2023). *Standard Test Methods for Notched Bar Impact Testing of Metallic materials* (ASTM Standard Version E23-18). <https://doi.org/10.1520/E0023-18>
- Babu, P. M., Rajamuneeswaran, S., Pritima, D., Marichamy, S., & Vairamuthu, J. (2020). Spark erosion machining behaviour of coconut shell ash reinforced silicon metal matrix. *Materials Today: Proceedings*, 33, 4602-4604. <https://doi.org/10.1016/j.matpr.2020.08.195>
- Bawa, M. A., Umaru, O. B., Abur, B. T., Salako, I., & Jatau, J. S. (2020). Effect of locust bean pod ash on the hardness and wear rate of heat treated A356 alloy metal matrix composite for production of automobile brake rotor. *International Journal of Research Publication (IJRP.ORG)*, 57(1), 36-43. <https://doi.org/10.47119/IJRP100571720201325>
- Bushlya, V., Lenrick, F., Gutnichenko, O., Petrusa, I., Osipov, O., Kristiansson, S., & Stahl, J.-E. (2017). Performance and wear mechanisms of novel superhard diamond and boron nitride based tools in machining Al-SiCp metal matrix composite. *Wear*, 376-377, 152-164. <https://doi.org/10.1016/j.wear.2017.01.036>
- Chak, V., Chattopadhyay, H., & Kumar, A. (2020). Synthesis , characterization and deformation of Al - 4.5Cu / SiCp composites. *Materials Today: Proceedings*, 26, 2833-2838. <https://doi.org/10.1016/j.matpr.2020.02.590>
- Chauhan, A., Vates, U. K., Kanu, J. N., Gupta, E., Singh, G. K., Sharma, B. P., & Gorrepati, S. R. (2021). Fabrication and characterization of novel nitinol particulate reinforced aluminium alloy metal matrix composites (NiTip/AA6061 MMCs). *Materials Today: Proceedings*, 38, 3027-3034. <https://doi.org/10.1016/j.matpr.2020.09.326>

- Das, D., Roy, D. K., Satpathy, M. P., Nanda, B. K., & Nayak, R. K. (2019). Compressive, impact and flexural behaviour of Al based metal matrix composites. *Materials Today: Proceedings*, 18(7), 3080-3086. <https://doi.org/10.1016/j.matpr.2019.07.180>
- Edhirej, A., Sapuan, S. M., Jawaid, M., & Zahari, N. I. (2017). Cassava / sugar palm fiber reinforced cassava starch hybrid composites : Physical , thermal and structural properties. *International Journal of Biological Macromolecules*, 101, 75-83. <https://doi.org/10.1016/j.ijbiomac.2017.03.045>
- Fang, X., Song, M., Li, K., & Du, Y. (2010). Precipitation sequence of an aged Al-Mg-Si alloy. *Journal of Mining and Metallurgy, Section B: Metallurgy*, 46(2), 171-180. <https://doi.org/10.2298/JMMB1002171F>
- Flanagan, S., Main, J., Lynch, P., Vanderwiel, C., & Roth, J. T. (2019). A mechanical evaluation of an overaged overaged aluminum metal-matrix-composite (2009 Al/SiC/15p MMC). *Procedia Manufacturing*, 34, 58-64. <https://doi.org/10.1016/j.promfg.2019.06.117>
- Fröck, H., Reich, M., & Milkereit, B. (2019). Scanning rate extension of conventional DSCs through indirect measurements. *Materials*, 12(7), Article 1085. <https://doi.org/10.3390/ma12071085>
- Geetha, B., & Ganesan, K. (2015). The effects of ageing temperature and time on mechanical properties of A356 aluminium cast alloy with red mud addition and treated by T6 heat treatment. *Materials Today: Proceedings*, 2(4-5), 1200-1209. <https://doi.org/10.1016/j.matpr.2015.07.032>
- Goudar, D. M., Srivastava, V. C., & Rudrakshi, G. B. (2018). Microstructure and mechanical properties of spray formed and hot pressed / heat treated Al- ( 20-30 wt %) Mg<sub>2</sub>Si-2 % Cu Alloy. *Research & Reviews: Journal of Material Sciences*, 6(1), 10-22. <https://doi.org/10.4172/2321-6212.1000211>
- Harussani, M. M., & Sapuan, S. M. (2022). Tensile and flexural properties of compression molded composites of epoxy reinforced with treated sugar palm fibre. *Journal of Natural Fibre Polymer Composites (JNFPC)*, 1(2), 1-13.
- Hashim, J., Looney, L., & Hashmi, M. S. J. (1999). Metal matrix composites: production by the stir casting method. *Journal of materials processing technology*, 92, 1-7. [https://doi.org/10.1016/S0924-0136\(99\)00118-1](https://doi.org/10.1016/S0924-0136(99)00118-1)
- He, H., Zhang, L., Li, S., Wu, X., Zhang, H., & Li, L. (2018). Precipitation stages and reaction kinetics of AlMgSi alloys during the artificial aging process monitored. *Metals*, 8(1), Article 39. <https://doi.org/10.3390/met8010039>
- Hiremath, A., & Hemanth, J. (2018). An exploratory study to evaluate the thermal conductivity of LM25-borosilicate glass (P) composites under the influence of different end chills. *Pertanika Journal of Science & Technology*, 26(4), 1837-1848.
- Ikubanni, P., Oki, M., Adeleke, A., Omoniyi, P., Ajisegiri, E., & Akinlabi, E. (2022). Physico-mechanical properties and microstructure response of hybrid reinforced Al6063 composites to PKSA/SiC Inclusion. *ACTA Metallurgica Slovaca*, 28(1), 25-32. <https://doi.org/10.36547/ams.28.1.1340>
- Ikumapayi, O. M., Afolalu, S. A., Bodunde, O. P., Ugwuoke, C. P., Benjamin, H. A., & Akinlabi, E. T. (2022). Efficacy of heat treatment on the material properties of aluminium alloy matrix composite impregnated with silver nano particle/calcium carbonate Al. *International Journal of Advanced Technology and Engineering Exploration*, 9(89), 523-535. <https://doi.org/10.19101/IJATEE.2021.874829>

- Ilyas, R. A., Sapuan, S. M., & Ishak, M. R. (2018). Isolation and characterization of nanocrystalline cellulose from sugar palm fibres (*Arenga Pinnata*). *Carbohydrate Polymers*, *181*, 1038-1051. <https://doi.org/10.1016/j.carbpol.2017.11.045>
- Ishak, M. R., Leman, Z., Sapuan, S. M., Rahman, M. Z. A., & Anwar, U. M. K. (2013). Impregnation modification of sugar palm fibres with phenol formaldehyde and unsaturated polyester. *Fibers and Polymers*, *14*(2), 250-257. <https://doi.org/10.1007/s12221-013-0250-0>
- Ishak, M. R., Sapuan, S. M., Leman, Z., Rahman, M. Z. A., Anwar, U. M. K., & Siregar, J. P. (2013). Sugar palm (*Arenga pinnata*): Its fibres, polymers and composites. *Carbohydrate Polymers*, *91*(2), 699-710. <https://doi.org/10.1016/j.carbpol.2012.07.073>
- Iyasele, E. O. (2018). Comparative analysis on the mechanical properties of a Metal-Matrix Composite (MMC) reinforced with palm kernel/periwinkle shell ash. *Global Scientific Journals*, *6*(8), 1-24.
- Kawin, N., Jagadeesh, D., Saravanan, G., & Periasamy, K. (2020). Optimization of turning parameters in sugarcane bagasse ash reinforced with Al-Si10-Mg alloy composites by Taguchi method. *Materials Today: Proceedings*, *21*, 474-476. <https://doi.org/10.1016/j.matpr.2019.06.634>
- Kennedy, Z. E., & Raja, A. I. (2022). Evaluation of mechanical properties of Al-B<sub>4</sub>C and Al-SiC metal matrix composites - A comparison. *Materials Today: Proceedings*, *55*, 380-383. <https://doi.org/10.1016/j.matpr.2021.08.356>
- Khan, A. H., Shah, S. A. A., Umar, F., Noor, U., Gul, R. M., Giasin, K., & Aamir, M. (2022). Investigating the microstructural and mechanical properties of novel ternary reinforced AA7075 hybrid metal matrix composite. *Materials*, *15*(15), Article 5303. <https://doi.org/10.3390/ma15155303>
- Kondoh, K., Kawakami, M., Imai, H., Umeda, J., & Fujii, H. (2010). Wettability of pure Ti by molten pure Mg droplets. *Acta Materialia*, *58*(2), 606-614. <https://doi.org/10.1016/j.actamat.2009.09.039>
- Kumar, K. R., Pridhar, T., & Balaji, V. S. S. (2018). Mechanical properties and characterization of zirconium oxide (ZrO<sub>2</sub>) and coconut shell ash (CSA) reinforced aluminium (Al6082) matrix hybrid composite. *Journal of Alloys and Compounds*, *765*, 171-179. <https://doi.org/10.1016/j.jallcom.2018.06.177>
- Lakshmikanthan, A., Prabhu, T. R., Babu, U. S., Koppad, P. G., Gupta, M., Krishna, M., & Bontha, S. (2020). The effect of heat treatment on the mechanical and tribological properties of dual size SiC reinforced A357 matrix composites. *Journal of Materials Research and Technology*, *9*(3), 6434-6452. <https://doi.org/10.1016/j.jmrt.2020.04.027>
- Li, N., Yan, H., & Wang, Z. W. (2018). Effects of heat treatment on the tribological properties of SiCp/Al-5Si-1Cu-0.5Mg composite processed by electromagnetic stirring method. *Applied Sciences*, *8*(3), Article 372. <https://doi.org/10.3390/app8030372>
- Lokesh, G. N., Prashanth, K. P., Prasad, G. P., & Venkatesha, B. K. (2022). Mechanical and microstructure evaluation of stir cast Al-4.5%Cu alloy reinforced fly ash/boron carbide hybrid metal matrix composites. *Materials Today: Proceedings*, *54*, 486-491. <https://doi.org/10.1016/j.matpr.2021.11.131>
- Mabuwa, S., Msomi, V., Ndube-Tsolekile, N., & Zungu, V. M. (2022). Status and progress on fabricating automotive-based aluminium metal matrix composites using FSP technique. *Materials Today: Proceedings*, *56*, 1648-1652. <https://doi.org/10.1016/j.matpr.2021.10.179>

- Manda, C. S., Babu, B. S., & Ramaniah, N. (2021). Effect of heat treatment on mechanical properties of aluminium metal matrix composite (AA6061/MoS<sub>2</sub>). *Advances in Materials and Processing Technologies*, 8, 205-222. <https://doi.org/10.1080/2374068X.2020.1860593>
- Manikandan, R., & Arjunan, T. V. (2019). Microstructure and mechanical characteristics of CDA-B4C hybrid metal matrix composites. *Metals and Materials International*, 27, 885-899. <https://doi.org/10.1007/s12540-019-00518-6>
- Mistry, J. M., & Gohil, P. P. (2019). Experimental investigations on wear and friction behaviour of Si<sub>3</sub>N<sub>4</sub>p reinforced heat-treated aluminium matrix composites produced using electromagnetic stir casting process. *Composites Part B: Engineering*, 161, 190-204. <https://doi.org/10.1016/j.compositesb.2018.10.074>
- Morampudi, P., Ramana, V. S. N. V., Bhavani, K., Reddy, C. K., & Vikas, K. S. R. (2022). Wear and corrosion behavior of AA6061 metal matrix composites with ilmenite as reinforcement. *Materials Today: Proceedings*, 52, 1515-1520. <https://doi.org/10.1016/j.matpr.2021.11.228>
- Nagaraja, S., Kodandappa, R., Ansari, K., Kurunian, M. S., Afzal, A., Kaladgi, A. A., Asliffattahi, N., Saleel, C. A., Gowda, A. C., & Anand, P. B. (2021). Influence of heat treatment and reinforcements on tensile. *Materials*, 14(18), Article 5261. <https://doi.org/10.3390/ma14185261>
- Nambiar, S., Adhikari, R., Upadhy, N., & Hande, R. (2020). Study on progressive wear of machine reamer while reaming Al6061/SiC Composite. *Pertanika Journal of Science & Technology*, 28(1), 403-420.
- Natrayan, L., Singh, M., & Kumar, M. S. (2017). An experimental investigation on mechanical behaviour of SiCp reinforced Al 6061 MMC using squeeze casting process. *International Journal of Mechanical and Production Engineering Research and Development*, 7(6), 663-668. <https://doi.org/10.24247/ijmperdddec201774>
- Olaniran, O., Uwaifo, O., Bamidele, E., & Olaniran, B. (2019). An investigation of the mechanical properties of organic silica, bamboo leaf ash and rice husk reinforced aluminium hybrid composite. *Material Science & Engineering International Journal*, 3(4), 129-134. <https://doi.org/10.15406/mseij.2019.03.00103>
- Olusesi, O. S., & Udoye, N. E. (2021). Development and characterization of AA6061 aluminium alloy/clay and rice husk ash composite. *Manufacturing Letters*, 29, 34-41. <https://doi.org/10.1016/j.mfglet.2021.05.006>
- Pasha, S. K., Sharma, A., & Tambe, P. (2022). Mechanical properties and tribological behavior of Al7075 metal matrix composites : A review. *Materials Today: Proceedings*, 56, 1513-1521. <https://doi.org/10.1016/j.matpr.2022.01.102>
- Patel, M., Sahu, S. K., Singh, M. K., & Dalai, N. (2022). Micro-structural and mechanical characterization of stir cast AA5052/B4C metal matrix composite. *Materials Today Proceedings*, 56, 1129-1136. <https://doi.org/10.1016/j.matpr.2021.10.331>
- Pasupulla, A. P., Amornphimoltham, P., Charles, P., Sundaram, V. S., & Ramakrishna, M. M. (2022). Taguchi L16 orthogonal array analysis on wear rate parameters for aluminum related hybrid composites. *Materials Today: Proceedings*, 62, 1692-1696. <https://doi.org/10.1016/j.matpr.2021.11.435>
- Rajaram, S., Subbiah, T., Mahali, P. K., & Thangara, M. (2022). Effect of age-hardening temperature on mechanical and wear behavior of furnace-cooled al7075-Tungsten Carbide compositer. *Materials*, 15(15), Article 5344. <https://doi.org/10.3390/ma15155344>
- Rajasekaran, S., Udayashankar, N. K., & Nayak, J. (2012). T4 and T6 Treatment of 6061 Al-15 Vol.% SiCP Composite. *ISRN Materials Science*, 2012, Article 374719. <https://doi.org/10.5402/2012/374719>

- Ramasamy, M., Daniel, A. A., & Nithya, M. (2021). Investigation on surface roughness of aluminium (Al7050/TiC/BN) hybrid metal matrix. *Materials Today: Proceedings*, 46, 852-856. <https://doi.org/10.1016/j.matpr.2020.12.852>
- Sabry, I., Ghafaar, M. A., Hamid, A., Mourad, I., & Idrisi, A. H. (2020). Stir casted SiC-Gr/Al6061 hybrid composite tribological and mechanical properties. *SN Applied Sciences*, 2, Article 943. <https://doi.org/10.1007/s42452-020-2713-4>
- Sajjadi, S. A., Ezatpour, H. R., & Beygi, H. (2011). Microstructure and mechanical properties of Al-Al<sub>2</sub>O<sub>3</sub> micro and nano composites fabricated by stir casting. *Materials Science and Engineering A*, 528(29-30), 8765-8771. <https://doi.org/10.1016/j.msea.2011.08.052>
- Sam, M., Radhika, N., & Sai, K. P. (2020). Effect of heat treatment on mechanical and tribological properties of aluminum metal matrix composites. *Proceedings of the Institution of Mechanical Engineers, Part C: Journal of Mechanical Engineering Science*, 234(22), 4493-4504. <https://doi.org/10.1177/0954406220922253>
- Samal, P., Vundavilli, P. R., Meher, A., & Mahapatra, M. M. (2020). Recent progress in aluminum metal matrix composites: A review on processing, mechanical and wear properties. *Journal of Manufacturing Processes*, 59, 131-152. <https://doi.org/10.1016/j.jmapro.2020.09.010>
- Seetharaman, S., Subramanian, J., Singh, R. A., Wong, W. L. E., Nai, M. L. S., & Gupta, M. (2022). Mechanical properties of sustainable metal matrix composites : A review on the role of green reinforcements and processing methods. *Technologies*, 10, Article 32.
- Shaikh, M. B. N., Arif, S., Aziz, T., Waseem, A., Shaikh, M. A. N., & Ali, M. (2019). Microstructural, mechanical and tribological behaviour of powder metallurgy processed SiC and RHA reinforced Al-based composites. *Surfaces and Interfaces*, 15, 166-179. <https://doi.org/10.1016/j.surfin.2019.03.002>
- Sharma, S., Nanda, T., & Pandey, O. P. (2019). Investigation of T4 and T6 heat treatment on the wear properties of sillimanite reinforced LM30 aluminium alloy composites. *Wear*, 426-427, 27-36. <https://doi.org/10.1016/j.wear.2018.12.065>
- Singh, B., Grewal, J. S., & Sharma, S. (2022). Effect of addition of flyash and graphite on the mechanical properties of A6061-T6. *Materials Today: Proceedings*, 50, 2411-2415. <https://doi.org/10.1016/j.matpr.2021.10.258>
- Singh, G., & Sharma, N. (2021). Study on the influence of T4 and T6 heat treatment on the wear behavior of coarse and fine WC particulate reinforced LM28 Aluminium cast composites. *Composites Part C: Open Access*, 4, Article 100106. <https://doi.org/10.1016/j.jcomc.2021.100106>
- Singh, K., Singh, H., Vardhan, S., & Mohan, S. (2022). An overview on the synthesis of aluminium matrix composites using stir casting technique. *Materials Today: Proceedings*, 60, 868-872. <https://doi.org/10.1016/j.matpr.2021.09.509>
- Singh, P., Gupta, R., Izan, S., Singh, S., Sharma, R., & Dwivedi, S. P. (2021). Tribo-mechanical behaviour of aluminium-based metal matrix composite: A review. *Materials Today: Proceedings*, 47, 3828-3832. <https://doi.org/10.1016/j.matpr.2021.03.092>
- Singh, V. K., Chauhan, S., Gope, P. C., & Chaudhary, A. K. (2015). Enhancement of wettability of aluminum based silicon carbide reinforced particulate metal matrix composite. *High Temperature Materials and Processes*, 34(2), 163-170. <https://doi.org/10.1515/htmp-2014-0043>

- Somashekhar, P. H., Sharma, K. V., & Girisha, H. N. (2018). Effect of heat treatment on tensile and hardness properties of Aluminium-7075 alloy reinforced with graphite and bagasse-ash composites. *IOSR Journal of Engineering*, 8(8), 38-43.
- Reddy, K. S. K., Kannan, M., Karthikeyan, R., Prashanth, S., & Reddy, B. R. (2020). A review on mechanical and thermal properties of aluminum metal matrix composites. *E3S Web of Conferences*, 184, Article 01033. <https://doi.org/10.1051/e3sconf/202018401033>
- Tiwari, K. S., Soni, S., Rana, R. S., & Singh, A. (2017). Effect of aging on mechanical behaviour of ADC12-fly ash particulate composite. *Material Today: Proceedings*, 4(2), 3513-3524. <https://doi.org/10.1016/j.matpr.2017.02.242>
- Varalakshmi, K., Kumar, K. C. K., Babu, P. R., & Sastry, M. R. C. (2019). Characterization of Al 6061-coconut Shell ash metal matrix composites using stir casting. *International Journal of Latest Engineering Science (IJLES)*, 2(3), 41-49. <http://ijlesjournal.org/2019/volume-2%20issue-3/ijles-v2i3p106.pdf>
- Velavan, K., Palanikumar, K., Natarajan, E., & Hong, W. (2020). Implications on the influence of mica on the mechanical properties of cast hybrid (Al+10%B4C+Mica) metal matrix composite. *Journal of Materials Research and Technology*, 10, 99-109. <https://doi.org/10.1016/j.jmrt.2020.12.004>
- Vencl, A., Bobic, I., Arostegui, S., Bobic, B., Marinković, A., & Babić, M. (2010). Structural, mechanical and tribological properties of A356 aluminium alloy reinforced with Al<sub>2</sub>O<sub>3</sub>, SiC and SiC+ graphite particles. *Journal of Alloys and Compounds*, 506(2), 631-639. <https://doi.org/10.1016/j.jallcom.2010.07.028>
- Venkatesh, L., Arjunan, T. V., & Ravikumar, K. (2019). Microstructural characteristics and mechanical behaviour of aluminium hybrid composites reinforced with groundnut shell ash and B4C. *Journal of the Brazilian Society of Mechanical Sciences and Engineering*, 41, Article 295. <https://doi.org/10.1007/s40430-019-1800-1>
- Xia, X., Zhao, Q., Peng, Y., Zhang, P., Liu, L., Ding, J., Luo, X., Huang, L., Zhang, H., & Chen, X. (2020). Precipitation behavior and mechanical performances of A356.2 alloy treated by Al-Sr-La composite refinement-modification agent. *Journal of Alloys and Compounds*, 818, Article 153370. <https://doi.org/10.1016/j.jallcom.2019.153370>
- Yang, K. V., Rometsch, P., Davies, C. H. J., Huang, A., & Wu, X. (2018). Effect of heat treatment on the microstructure and anisotropy in mechanical properties of A357 alloy produced by selective laser melting. *Materials & Design*, 154, 275-290. <https://doi.org/10.1016/j.matdes.2018.05.026>
- Yashpal, Sumankant, Jawalkar, C. S., Verma, A. S., & Suri, N. M. (2017). Fabrication of aluminium metal matrix composites with particulate reinforcement: A review. *Materials Today: Proceedings*, 4(2), 2927-2936. <https://doi.org/10.1016/j.matpr.2017.02.174>
- Yuan, D., Yang, X., Wu, S., Lü, S., & Hu, K. (2019). Development of high strength and toughness nano-SiCp/A356 composites with ultrasonic vibration and squeeze casting. *Journal of Materials Processing Technology*, 269, 1-9. <https://doi.org/10.1016/j.jmatprotec.2019.01.021>
- Yuan, Q., Fu, D., Zeng, X., & Liu, Y. (2017). Fabrication of carbon nanotube reinforced AZ91D composite with superior mechanical properties. *Transactions of Nonferrous Metals Society of China*, 27(8), 1716-1724. [https://doi.org/10.1016/S1003-6326\(17\)60194-8](https://doi.org/10.1016/S1003-6326(17)60194-8)